Metabolic modeling of a plant-pathogen interaction quantifies the metabolic bottlenecks underlying bacterial wilt

Léo Gerlin[1,2], Stéphane Genin[1], Caroline Baroukh[1]*

[1]LIPME, Université de Toulouse, INRAE, CNRS, Castanet-Tolosan, France

[2]INRAE, INSA Lyon, BF2I, UMR203, 69621 Villeurbanne, France

*Corresponding author: caroline.baroukh@inrae.fr

ORCID: 0000-0002-1041-1730 (CB)

ORCID: 0000-0003-2498-2400 (SG)

ORCID: 0000-0002-1398-2790 (LG)

Keywords

Genome-scale metabolic model; plant-pathogen interaction; tomato; *Ralstonia solanacearum;* putrescine

Short title

Metabolic bottlenecks of bacterial wilt

Abstract

During plant infection, complex metabolic interactions take place between the plant and the pathogen, among which occurs a true battle for resources. On one side, the pathogen harvests nutrients at the expense of the plant to sustain its growth and virulence. On the other side, the plant tries to prevent pathogen multiplication by competing for nutrients or using anti-microbial compounds. Plants and pathogens have thus contrary objectives in an intertwined system that is particularly difficult to untangle experimentally. To help decipher this interaction, we used genome-scale metabolic modeling by combining a multi-organ model of a plant, a model of a pathogen, quantitative data and a mathematical approach using sequential flux balance analyses (FBAs). We applied this modeling strategy to the interaction between the pathogenic bacterium *Ralstonia pseudosolanacearum* and its natural host, the tomato plant. This allowed, for the first time, quantitative modeling of the fluxes of matter occurring during plant infection. The model showed that, for the pathosystem studied, i) the plant's photosynthetic capacity is a more stringent environmental condition than minerals for bacterial proliferation ii) reduction of the plant transpiration is what limits and then stops plant growth and later pathogen growth, iii) hijacking stem resources can boost bacterial growth but is accessory, and iv) pathogen-excreted putrescine is predicted to be directly reused for plant biomass. This study provides the first holistic and quantitative view of a plant-pathogen interaction, and highlights the criticality of water flow when the bacteria responsible of the infection is a fast-growing, xylem-colonizing one.

Introduction

Metabolism is a determining parameter at the center of interactions between plants and pathogens. Indeed, during host infection, pathogens must efficiently find resources in hostile (and sometimes nutrient-poor) environments to sustain both their growth and virulence (Abu Kwaik & Bumann, 2013). This implies a trade-off for the infecting pathogen, which must balance its carbon and energy expenditure between two objectives: on one hand, limiting plant defense and hijacking plant resources, and on the other hand, supporting its own multiplication and proliferation (Berger et al., 2007). On the plant side, a similar trade-off exists where the plant must distribute resources between maintenance/growth (to ensure reproduction) and immunity, while coping with an increasing infecting population that affects its physiology (Herms & Mattson, 1992; Walters & Heil, 2007). Understanding this complex metabolic interaction between the plant and the pathogen is necessary to gain a more holistic view of the infection process. However, several challenges complicate this understanding: i) the difficulty in distinguishing pathogen metabolism from plant metabolism, except for very specific metabolites, and ii) the dynamic interplay of multiple synthesis and degradation processes. These factors prevent the use of a simple metabolomic comparison between infected and non-infected plants. To better tackle this interaction, a systemic and computational approach is necessary.

To address these challenges, genome-scale metabolic models (GSMM) could be used. GSMMs integrate the metabolic potential of an organism of interest, encompassing thousands of metabolic reactions based on genomics, physiological and biochemical evidences. These models can quantitatively predict the flux of matter in the biological system studied (Gu et al., 2019) as well as phenotypic parameters such as growth. GSMMs have repeatedly proven to be pertinent tools for unraveling complex metabolism and understanding it quantitatively, making them suitable for elucidating plant - pathogen metabolic interactions (Gerlin, Frainay, et al., 2021).

Recently, genome-scale metabolic modeling has been applied to the plant – pathogen system of tomato and *Phytophthora infestans* (Rodenburg et al., 2019). However, this study was qualitative rather than quantitative. A quantitative model of the plant – mutualist symbiont system *Medicago truncatula* - *Sinorhizobium meliloti* has also been recently developed (Pfau et al., 2018; diCenzo et al., 2020). Yet modeling a pathogenic interaction, as compared to a mutualistic one, raises additional methodological

75 questions: i) the choice of the objective function (i.e. the flux(es) to minimize/maximize)
76 in an antagonistic relationship, given that the modeling approach assumes an optimal
77 behavior of the biological system; ii) the need for extensive data acquisition, including
78 the plant/pathogen ratio, growth rates, and metabolites available for the pathogen.
79 These considerations are crucial for developing accurate, meaningful and quantitative
80 models of plant-pathogen interactions.

81 In this study, we constructed the first quantitative genome-scale metabolic model of a
82 plant–pathogen interaction. For our model pathosystem, we used *Ralstonia*
83 *pseudosolanacearum* GMI1000 and its natural host, the tomato plant. *R.*
84 *pseudosolanacearum* is a bacterial plant pathogen that has been extensively studied
85 for its virulence factors (Vailleau & Genin, 2023) and has gained growing attention for
86 the metabolic aspects of its lifestyle (Peyraud et al., 2016; Lowe-Power et al., 2018;
87 Lowe-Power et al., 2018; Peyraud et al., 2018; Hamilton et al., 2021; Gerlin, Escourrou,
88 et al., 2021). It was among the first plant pathogens having a high-quality genome scale
89 metabolic model published (Peyraud et al., 2016). *R. pseudosolanacearum* is a soil-
90 borne beta-Proteobacterium that enters plants through roots to reach the vascular
91 tissues. The pathogen is then able to reach aerial parts, and proliferate dramatically in
92 xylem vessels, which are typically considered nutrient-poor environments (De La
93 Fuente et al., 2022). Bacterial density has been identified as for the cause of xylem
94 vessel clogging (Ingel et al., 2022), leading to lethal wilting symptoms. A progressive
95 growth arrest of the plant has also been observed (Gerlin, Escourrou, et al., 2021). The
96 tomato, *R. pseudosolanacearum*'s natural host, has also been part of the recent
97 growing importance of metabolic models in plants (Gerlin, Frainay, et al., 2021): a cell
98 genome-scale metabolic model was originally published in 2016 (Yuan et al., 2016)
99 and a genome-scale multi-organ metabolic model, with particular emphasis on xylem
100 vessels (where *R. pseudosolanacearum* is most metabolically active), was recently
101 published (Gerlin et al., 2022). A core metabolic model of tomato stem in the context
102 of a fungal infection has also been published (Lacrampe et al., 2024).

103 In this study, we developed a quantitative genome-scale metabolic model of *R.*
104 *pseudosolanacearum* – tomato plant interaction, named VIRION (VIrtual Ralstonia-
105 tomato plant interactION). This model is based on the multi-organ metabolic model of
106 the tomato plant, representing different plant organs during vegetative growth (leaf,
107 stem, root with xylem and phloem as exchange compartments), and *R.*

108 *pseudosolanacearum* was added as an additional compartment connected to the
109 xylem. To accurately simulate the antagonistic interaction between the plant and the
110 pathogen, we employed a set of sequential Flux Balance Analyses (FBAs). VIRION
111 also integrates a comprehensive set of physiological and metabolic data: i) tomato
112 vegetative growth (organ ratio, growth rates, xylem metabolites), ii) tomato infection by
113 *R. pseudosolanacearum* (plant/pathogen ratios, impacts of infection on physiology),
114 and iii) *R. pseudosolanacearum* physiology and metabolic capacities (growth rates,
115 assimilation and excretion capacities on xylem metabolites). We did not explicitly
116 model the role of immunity in the interaction because such modeling relies instead on
117 other approaches (such as dynamic gene regulatory networks or functional association
118 networks) (Windram et al., 2014) and therefore requires specific datasets. Our
119 approach here was to focus on the trophic relationship between the host and the
120 pathogen at a stage which, in the case of Ralstonia, corresponds to strong
121 multiplication within the plant tissues, and thus likely occurs when most of the immunity
122 has already been overcome (Gerlin, Escourrou, et al., 2021; Baroukh et al., 2024). This
123 stage of the interaction has been rather little studied until now, whereas there are
124 numerous studies on early plant immunity (perception and signaling) (DeFalco & Zipfel,
125 2021; Jian et al., 2023).

126 The model enables the predictions of the growth capacities of *R. pseudosolanacearum*
127 *in planta* at different stages of the disease, as well as the pathogen's impact on plant
128 growth and metabolism. We used the model to analyze factors causing the infected
129 plant to cease growth and those limiting bacterial growth. Finally, we also investigated
130 potential hijacking of stem resources during the disease, and the fate of the bacterial
131 excreted putrescine in the plant.

132

Results

Modeling an antagonist plant-pathogen interaction using a multi-compartment metabolic model and sequential Flux Balance Analyses

To quantitatively model the metabolic interaction between *R. pseudosolanacearum* and tomato, we formalized this interaction as a system composed of four metabolic compartments encompassing the main metabolic roles of the plant (leaf, stem, root) and the pathogen. Metabolites can be exchanged between these compartments through xylem and phloem (Figure 1A). Each of these four compartments was represented as a genome-scale metabolic model: iRP1476 for the pathogen (Peyraud et al., 2016) and Sl2183 for the plant compartments (Gerlin et al., 2022) (Figure 1B), with minor modifications as reported in the Methods section. As in Gerlin et al. (2022), the physiological roles of each compartment (described in Figure 1A) were considered as FBA constraints (Figure 1B). In brief: i) minerals and water can only enter the system through the root and are routed to the higher parts of the plant and to the pathogen only via xylem, ii) photons are assimilated in leaf and stem, with higher efficiency in the leaf, iii) the carboxylase/oxygenase activity of the Rubisco was constrained to experimentally measured value. For a complete description and justification of these constraints, readers are referred to Gerlin et al. (2022).

FBA is an approach based on an optimization problem (typically linear programming), where one or several reactions must be maximized or minimized to compute fluxes of matter (Orth et al., 2010). Usually, when modeling ecosystems, it is assumed that the organisms composing the system maximize global biomass (diCenzo et al., 2020). However, this assumption is not reasonable for our antagonist system, where the pathogen grows at the expense of the plant, implying decoupled growth between the plant and the pathogen. Additionally, in our system, the metabolic composition of xylem sap is severely affected upon bacterial infection, particularly at high bacterial densities (Gerlin, Escourrou, et al., 2021), questioning the quasi-steady state assumption (QSSA). To accurately model this antagonistic relationship, we used a system of sequential FBAs (Figure 1C). In this approach, an initial FBA determines one or several optimal flux(es). These fluxes are subsequently reinjected into a following FBA as an additional constraint. A total of 4 successive FBAs were performed for a given bacterial density to predict both bacterial and plant metabolism during the interaction. We

166 repeated this 4-FBA resolution workflow for several bacterial densities representative
167 of those found *in planta*. This was achieved by changing the plant/pathogen ratio
168 through exchange coefficients in the uptake and production reactions between the
169 xylem and the pathogen.

170 The sequential 4-FBA approach consisted of the four following steps:

171 FBA 1: estimation of the requirements of a healthy plant in terms of photons, nitrogen
172 and other minerals for optimal growth of leaf, stem and root.

173 FBA 2: optimization of pathogen growth while limiting plant photon input and optionally
174 mineral inputs to those obtained in FBA 1. This ensured that resource usage did not
175 exceed that of a healthy plant. Photon constraints were always applied, while iron,
176 nitrogen or other minerals constraints were optional. Additionally, transpiration flow,
177 which is significantly reduced after pathogen inoculation (Gerlin, Escourrou, et al.,
178 2021) and affects xylem exchanges, could be constrained at this step.

179 FBA 3: integration of the pathogen's maximal growth obtained in FBA 2 as a constraint,
180 while maximization of leaf and stem growth. This step estimated the plant's capacity to
181 continue growth under the pathogen's metabolic activities. In both FBA 2 and FBA 3,
182 root growth rate was constrained to experimentally observed values, as root growth is
183 minimally affected by pathogen colonization of xylem vessels according to
184 experimental data on infected tomato plants (Gerlin, Escourrou, et al., 2021).

185 FBA 4: minimization the sum of absolute fluxes while constraining leaf and stem growth
186 rate to the optimal values obtained in FBA 3. This step represented a parsimonious
187 enzyme usage by both the pathogen and the plant. This final simulation yielded the
188 fluxes of matter and phenotype prediction (pathogen and plant growth) for a given
189 bacterial density. By performing these 4 FBAs for bacterial densities ranging from 10^4
190 to 10^{12} Colony Forming Unit per gram of Fresh Weight (CFU/gFW), we captured all
191 features of the plant-pathogen interaction during an infection. The simulation results
192 were compared to experimental biological values to gain insights into the pathosystem.

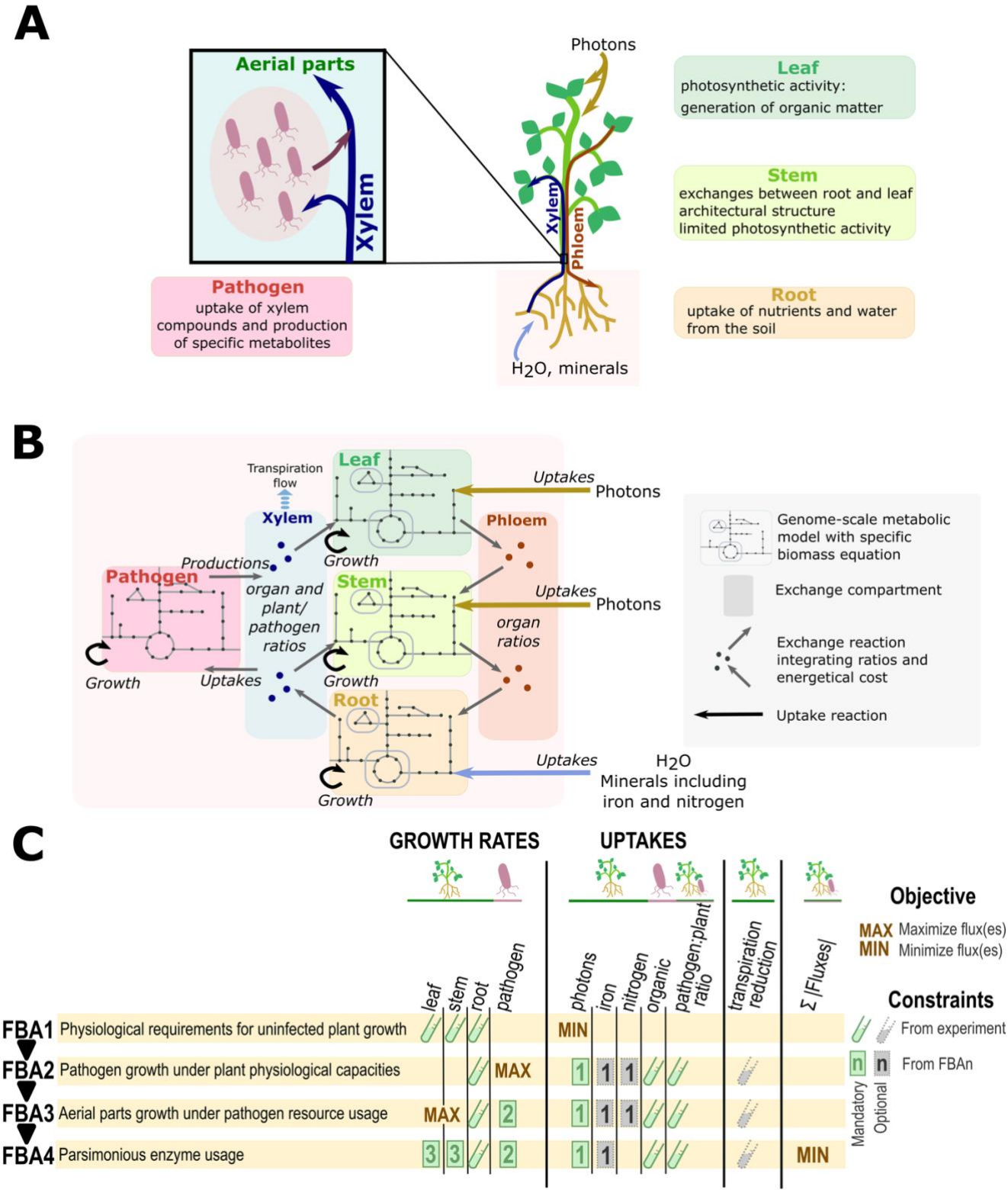

Figure 1: Schematic representation of the metabolic model VIRION

A. The main components of the system modeled in this study. Leaf, stem, root and the pathogen are each represented by a genome-scale metabolic model. Xylem and

197 phloem are exchange compartments. Inputs of the system are photons, connected to
198 leaf and stem, and water and minerals, connected through the root.

199 B. Schematic representation of the multi-compartment model and quantitative
200 approach developed in this study. Arrows represent relationships between the different
201 organs and the possible quantitative constraints which can be set in the model (growth,
202 uptakes, exchanges, transpiration flow).

203 C. Sequential Flux Balance Analyses (FBAs). Schematic representation of the different
204 FBAs solved in a sequential approach to obtain a phenotype prediction of the
205 pathosystem (growth rate of plant organs and pathogen) as well as fluxes of matter.
206 The constraints from experiments are explicated in Supplementary Table 1.

207

Identifying metabolic bottlenecks during the plant – pathogen interaction

We used the VIRION model to estimate the most limiting plant environmental factor (bottleneck) constraining the plant – pathogen interaction. Our analysis focused on the effect of nitrogen, iron and transpiration as individual limitations or as combined constraints (Figure 2A). We considered photon limitation as mandatory since an infected plant could not increase its photons uptake. Indeed, the leaf area of an infected plant was similar or less than the one of a healthy plant (Gerlin et al., 2022). While other minerals could be tested, our study focused on nitrogen and iron, which are particularly emphasized in the literature. Indeed nitrogen source influences the concentration of xylem organic metabolites in tomato (Bialczyk et al., 2004), while both iron and nitrogen are suggested to influence bacterial switch to virulence in *R. pseudosolanacearum* (Bhatt & Denny, 2004; Dalsing & Allen, 2014; Dalsing et al., 2015). Iron and nitrogen limitations were implemented as constrained iron and nitrogen uptake rate in FBA 2 (maximizing pathogen growth, Figure 1C), which could not exceed those inferred from FBA 1 (minimization of plant photons for a healthy tomato plant, Figure 1C). In FBA 2, transpiration could also be limited in a proportional manner depending on the bacterial density using a previously determined linear relationship between *in planta* bacterial density and transpiration reduction established in Gerlin et al. (2021) (see Methods for further details).

When photon availability is the sole limiting factor (Figure 2), which constrains photosynthesis and organic carbon production within the plant, *R. pseudosolanacearum* can grow at its maximal rate in the plant until a density of $10^{9.7}$ CFU/gFW (Figure 2B). Bacterial growth is then strongly reduced, reaching less than 0.05 h^{-1} when bacterial density exceeds $10^{10.6}$ CFU/gFW. We conclude here that plant carbon resources cannot support bacterial growth at higher density than 10^{10} CFU/gFW if bacteria growth relies solely on biotrophy.

Based on *in planta* analyses and *in vitro* assays on a mixture of substrates, glutamine has been characterized as the main carbon source of *R. pseudosolanacearum* in tomato xylem sap (Baroukh et al., 2022; Gerlin, Escourrou, et al., 2021; Baroukh et al., 2024). Our simulation results showed high glutamine uptake by *R. pseudosolanacearum* (Figure 2D), limited only by the bacterium's maximal uptake rate. At very high bacterial density, close to 10^{10} CFU/gFW, glutamine became insufficient

241 for both aerial part and bacterial growth, reaching the maximal allowed glutamine flux
242 (Figure 2E), based on measurement for a healthy plant. This primarily impaired aerial
243 parts growth, leading to a decline and then arrest of plant growth (Figure 2C), followed
244 by limited *R. pseudosolanacearum* glutamine uptake and growth capacity. The
245 glutamine limitation was slightly compensated by glucose uptake, a secondary carbon
246 source co-consumed with glutamine. While glucose can moderately contribute to
247 bacterial proliferation, it remains accessory (Baroukh et al., 2022, 2024; Gerlin,
248 Escourrou, et al., 2021; Hamilton et al., 2021). At slightly higher densities ($10^{10.25}$
249 CFU/gFW), the maximal glucose uptake flux in xylem was also reached (Figure 2G),
250 further limiting bacterial growth (Figure 2F). This accessory role of glucose can also be
251 inferred from its fluctuating uptake rates at low density (Figure 2G), showing that
252 glucose uptake is not a limiting factor at low density when the growth of Ralstonia is
253 maximized, unlike glutamine.

254 When comparing simulation results with only photon limitation to experimental data,
255 plant physiological capacities were overestimated. Simulations showed optimal leaf
256 and stem growth until a bacterial density of $10^{8.5}$ CFU/gFW (Figure 2C), whereas
257 experimentally, a strong effect on plant growth occurred between 10^6 and 10^8
258 CFU/gFW (Gerlin, Escourrou, et al., 2021). This suggests that other factors are
259 involved in the observed plant growth arrest. When minerals constraints (iron and
260 nitrogen) were applied, separately or together, no additional effect was visible on plant
261 and pathogen growths (Figure 2B and 2C) or metabolic exchanges (Figure 2D-G). This
262 implies that nitrogen and iron were less stringent bottlenecks than carbon in the
263 interaction. Replacing mineral constraints with a transpiration flow constraint resulted
264 in a more drastic and earlier impact on growths (Figure 2B and 2C) and metabolic
265 exchanges (Figure 2D-G). Reduction of transpiration, starting at 10^7 CFU/gFW,
266 immediately limited xylem contents available for bacteria and aerial parts. Our
267 sequential FBAs assumed that access to nutrients favors bacterial growth at the
268 expense of plant growth. Consequently, the effect of transpiration limitation was
269 immediate on plant growth (Figure 2C), which had access to less nitrogen.
270 Transpiration limitation alone thus seems sufficient to provoke plant growth decline and
271 eventual arrest. Following the impact on plant growth, xylem fluxes became insufficient
272 to sustain the maximal growth rate of *R. pseudosolanacearum*, causing a switch to an
273 intermediate growth rate (Figure 2B). However, xylem metabolites remained abundant

enough to sustain this intermediate growth rate for several higher bacterial densities, as *R. pseudosolanacearum* can co-assimilate many available carbon sources (Baroukh et al., 2022, 2024).

Interestingly, up to 10^9 CFU/gFW, glutamine remained abundant enough to satisfy the glutamine maximal uptake rate of *R. pseudosolanacearum*. Other metabolites present at scarce concentrations in xylem, such as glucose (Figure 2F), sucrose and other amino acids (Supplementary Figure 1), were no longer assimilated or assimilated at reduced rate. Beyond 10^9 CFU/gFW, glutamine became insufficient for bacteria, strongly impairing its growth and leading rapidly to growth arrest. These findings align with experimental data, where the maximal CFUs are around 10^9 CFU/gFW (Gerlin, Escourrou, et al., 2021). They also corroborate with a recently developed macroscopic model of *R. pseudosolanacearum* growth *in planta* (Baroukh et al., 2024).

Finally, adding nitrogen and iron limitations to the model, which was already constrained by photons and transpiration, did not significantly alter the effect on disease progression (Figure 2B-G). This finding implies that the decline in transpiration of the plant, which reduces xylem fluxes, has the strongest effect on both plant and pathogen metabolic capacities. Transpiration decline thus seems to be the most probable mechanism behind plant growth arrest, pathogen growth arrest and maximal bacterial density. In contrast, limitations of nitrogen, iron and carbon (through photons) do not appear to be the primary mechanisms behind these experimental observations.

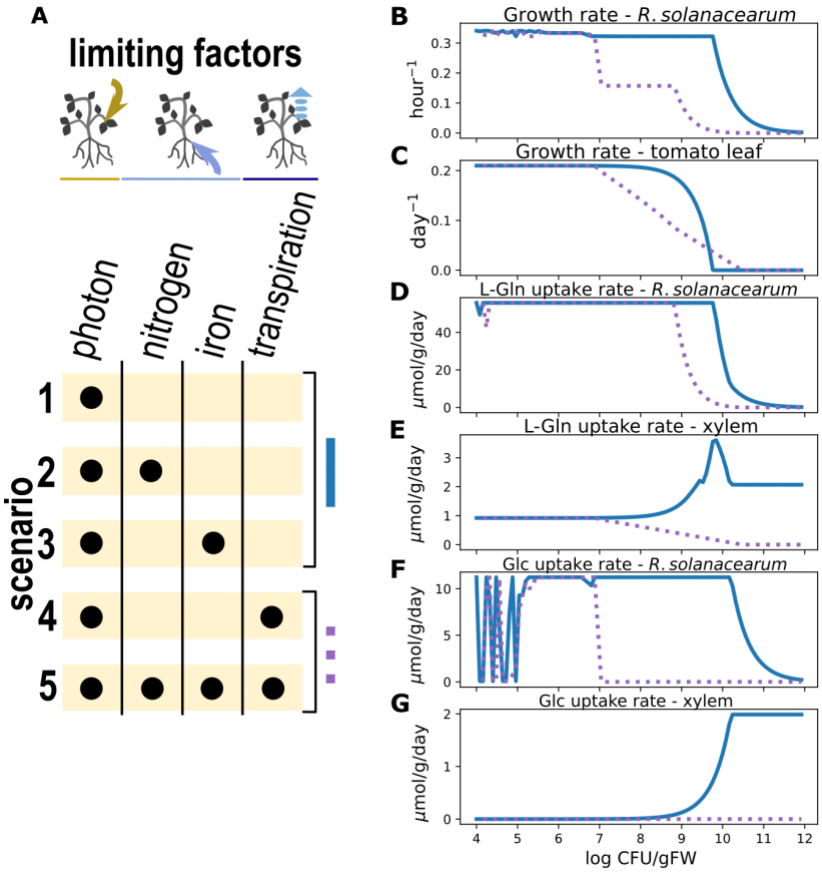

Figure 2: Effect of limiting plant environmental conditions on growth and metabolic exchanges. A. Simulation scenarios in which different plant environmental conditions are constrained at FBA 2 step during sequential FBAs. Photons, nitrogen and iron limitation constraints are set to the values obtained from resolution of FBA 1 while the transpiration limit is derived from experimental values (Gerlin, Escourrou, et al., 2021). B. to G. Effects of limiting factors on growth or exchanges for bacterial densities ranging from 10^4 to 10^{12} CFU/gFW. g means g of respectively *R. pseudosolanacearum* dry weight (D., F.) and root dry weight (E., G.). L-Gln: L-Glutamine, Glc: D-glucose, CFU: colony forming units, FW: fresh weight.

306 ## Quantitatively assessing the pathogen's strategy of hijacking tomato
307 stem resources

308 In the previous simulations, contribution of stem to xylem sap was forbidden. This is
309 consistent with the fact that no flux from stem to xylem was found by simulation for a
310 healthy plant (Gerlin et al., 2022). However, it can be argued that these fluxes could
311 appear in an infected tomato plant and thus contribute to pathogen nutrition if the
312 pathogen uses a host resource hijacking strategy. This would align with the hypothesis
313 that some type 3 secretion effectors of *R. pseudosolanacearum* modify plant
314 metabolism (Landry et al., 2020; Macho, 2016). We re-modeled scenario #5 from the
315 previous section (where photons, nitrogen, iron, transpiration are all limited, Figure 2A)
316 but this time export of nutrients from stem to xylem was authorized (Figure 3A),
317 creating scenario #6. Simulation results showed that allowing the stem to enrich xylem
318 sap had a slight effect on tomato leaf growth (Figure 3C). However, a more important
319 effect on pathogen growth was observed (Figure 3B). Indeed, *Ralstonia* could maintain
320 a maximal growth rate until $10^{9.2}$ cells per g of fresh weight instead of 10^{7} in scenario
321 #5, comparable to scenarios #1, #2 and #3 for which no transpiration limit was imposed
322 (Figure 3B). The possibility to sustain a maximal growth rate at higher densities was
323 due to the enrichment of xylem sap in glucose, sucrose and amino acids, thanks to the
324 stem's contribution (Figure 3D, Figure 2, Supplementary Figure 1). Nutrients from the
325 stem thus counterbalanced the effect of reduced transpiration flow and allowed *R.*
326 *pseudosolanacearum* growth to reach higher densities. However, the capacity of the
327 pathogen to induce such significant rewiring of the stem flux can be questioned in the
328 light of experimental data. Bacterial population dynamics *in planta* experimentally
329 measured in Gerlin et al. (2021) showed a near-stop of bacterial growth at
330 approximately 10^{9} CFU/gFW. This aligns more closely with scenario #4 or #5 (without
331 hijacking of stem resources) than with scenario #6.

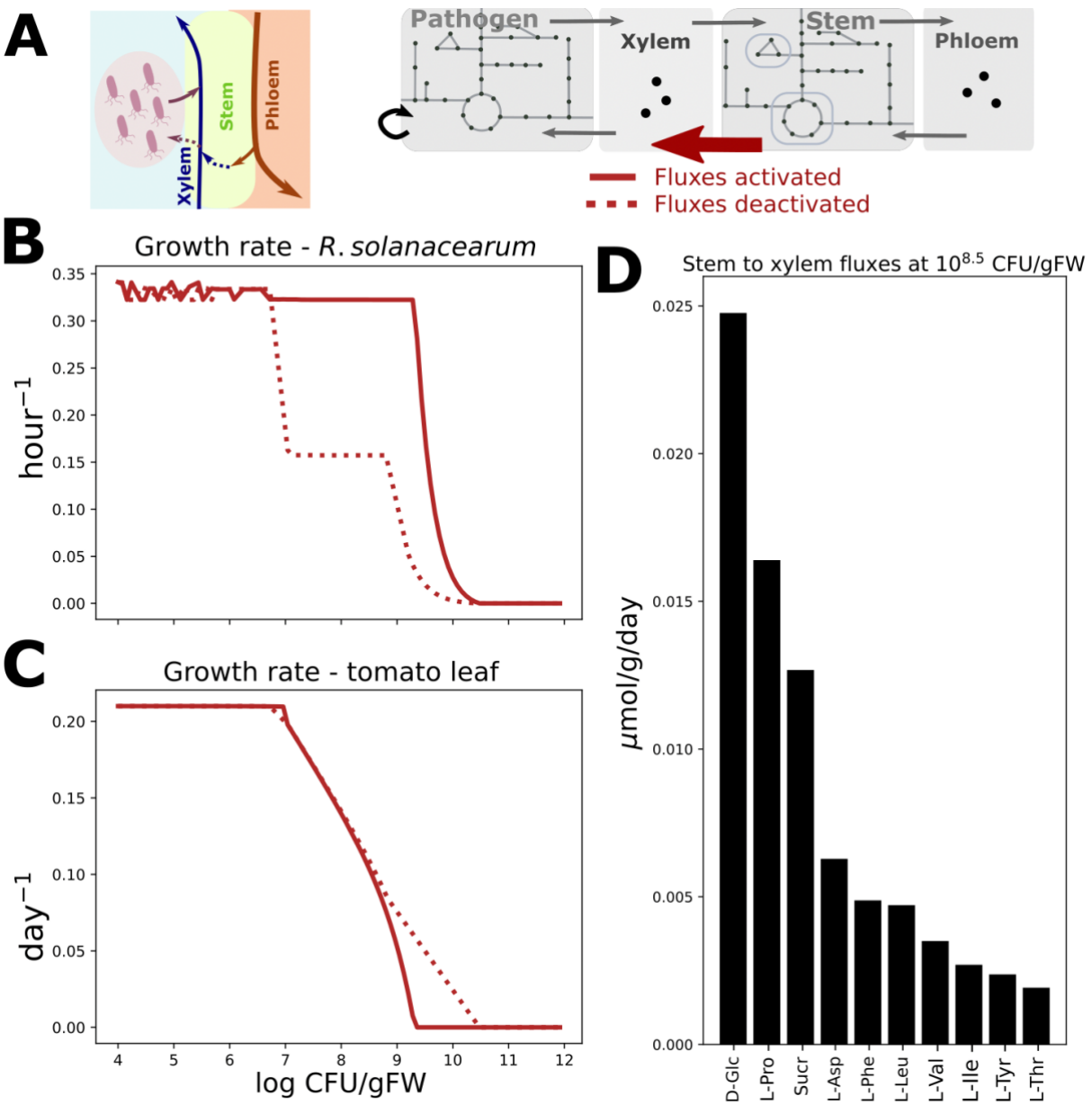

Figure 3: Effect of stem xylem sap enrichment on plant growth, pathogen growth and xylem sap composition. A. Schematic representation of the investigated plant fluxes. In scenarios #1 to #5, the stem could not enrich xylem sap. This rule was lifted to see the effect on the pathosystem metabolism. B. Pathogen growth rate when the stem can (dotted line) or cannot (line) enrich xylem sap. C. Plant growth rate when the stem can (dotted line) or cannot (line) enrich xylem sap. D. Fluxes of matter from stem to xylem when the stem can enrich xylem sap. g means g of stem dry weight. Fluxes were computed for a bacterial density of $10^{8.5}$ CFU/gFW. Fluxes are 0 when stem cannot enrich xylem sap. D-Glc: D-Glucose, L-Pro: L-Proline, Sucr: sucrose, L-Asp: L-Aspartate, L-Phe: L-Phenylalanine, L-Leu: L-Leucine, L-Val: L-Valine, L-Ile: L-Isoleucine, L-Tyr: L-Tyrosine, L-Thr: L-Threonine.

344 ## The fate of putrescine in the *Ralstonia*-tomato interaction

345 Putrescine fate during plant – *R. pseudosolanacearum* interaction is frequently
346 questioned, as putrescine is abundantly produced by the bacterium *in vitro* and *in*
347 *planta* (Gerlin, Escourrou, et al., 2021; Lowe-Power et al., 2018; Peyraud et al., 2016)
348 and contributes to virulence by accelerating wilt symptoms (Lowe-Power et al., 2018).
349 We analyzed the predicted fluxes in our model between putrescine production by *R.*
350 *pseudosolanacearum*, quantitatively calibrated to its experimental putrescine excretion
351 rate in a xylem-mimicking media (Baroukh et al., 2024), and its assimilation by the
352 plant, at a low and a high bacterial density ($10^{6.5}$ and $10^{8.5}$ cells per g of fresh weight)
353 (Figure 4A). When putrescine is produced by the bacterium from ornithine, a small
354 portion is incorporated into the bacterial biomass, while the majority is exported to
355 xylem, following a previously characterized excretion rate (Baroukh et al., 2022, 2024;
356 Peyraud et al., 2016). Subsequently, the plant stem has the capacity to assimilate part
357 of this excreted putrescine. Some of the metabolic reactions associated with putrescine
358 degradation were inactivated in our model, such as its conversion into N-
359 acetylspermidine (N1-acetylspermidine oxidase, identifier R_RE1537C in the model)
360 or into N-Methylputrescine (Putrescine N-methyltransferase, R_PMT), since these
361 fluxes would lead to dead-end metabolites not connected to central metabolism. Our
362 model predicted that at low bacterial density, all putrescine is converted into 4-
363 aminobutanal and then into gamma-Aminobutyric acid (GABA). The amount of GABA
364 produced from putrescine at this bacterial density is inferior to the stem biomass
365 requirements for GABA, which is supplemented by other reactions producing it from
366 glutamate (glutamate decarboxylase, R_GUDC, 4.1.1.15). At high bacterial density,
367 GABA production from putrescine exceed the stem biomass requirements. This excess
368 of incoming putrescine is compensated by the activation of: i) the pathway allowing the
369 incorporation of GABA into TCA cycle through GABA shunt (transport into
370 mitochondria (R_4abut_tx_m_) and conversion into succinate-semialdehyde (4-
371 aminobutyrate transaminase, R_ABTArm) in the stem, ii) the activation of the pathway
372 allowing conversion of putrescine into GABA and assimilation in biomass in the leaf.
373 Interestingly, excess putrescine assimilated by the plant through GABA involves the
374 mandatory production of hydrogen peroxide (H_2O_2) (Figure 4B), a modulator of redox
375 homeostasis (Gerlin, Baroukh, et al., 2021), particularly in stem. The production of
376 hydrogen peroxide in stem follows the pathogen growth, and peaks at 10^9 cells per g

377 of fresh weight. At higher densities, the limited capacities of the pathogen to pursue its
378 growth impacts putrescine production flux, thus reducing hydrogen peroxide flux.

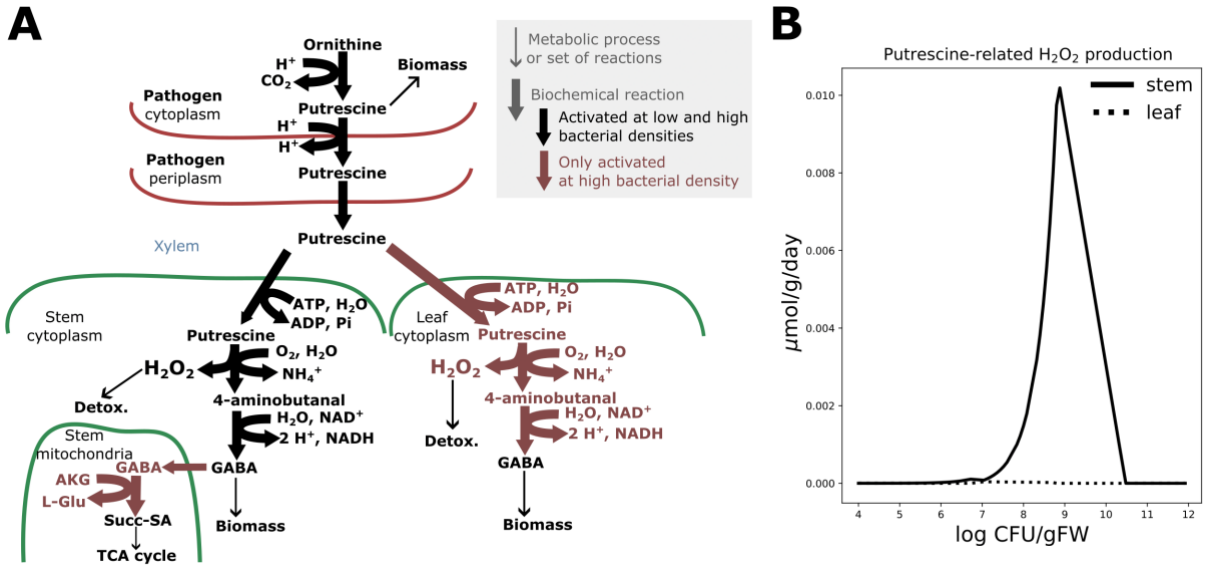

Figure 4: Fluxes predictions surrounding putrescine in VIRION. Only fluxes activated between putrescine production by the pathogen and its complete assimilation by the plant are represented. In B, g means g of stem (full line) or leaf (dotted line) dry weight.

Discussion

Modeling a plant-pathogen interaction using Flux Balance Analysis

FBA is a methodology widely used in the systems biology community because of its simplicity to set up, its capacity to model at the genome-scale level and its relatively low number of parameters to calibrate (Orth et al., 2010). However, this methodology relies on the quasi-steady-state assumption (QSSA), assuming that no internal metabolites of the system accumulate or get depleted, as well as the fact that the system is optimal with respect to an objective (most often assumed to be growth). The difficulty in modeling a plant-pathogen system lies in the fact that the pathogen grows at the expense of the plant, implying antagonistic objectives between the organisms composing the system. Therefore, questions arise regarding the choice of the objective function that should be optimized. In addition, the pathogen might deplete or accumulate some metabolites upon its growth in the plant, which probably challenges the QSSA.

As a first approximation to quantitatively model a plant-pathogen interaction, we proposed in this work a methodological framework consisting of solving, for several bacterial densities, 4 sequential FBA models in which each FBA model is constrained by the optimal value of the previously solved FBA. In this methodology, we thus assumed that for each bacterial density inside the plant, the internal metabolites were “at steady-state”. We also assumed that pathogen growth was at the expense of the aerial parts of the plant. Despite these strong hypotheses, VIRION was able to illustrate its relevance by predicting growth rates of the aerial part of the plant and the pathogen close to what was experimentally observed. VIRION also allowed to dissect novel and yet unquantified aspects of the *R. pseudosolanacearum* – tomato interaction, such as the importance of the transpiration decline and its implication in plant growth arrest, the importance of carbon compared to other elements and the relative importance of stem resource hijacking.

As future directions, the model could be used to study the impact of plant environmental conditions on the plant-pathogen interaction or extended to consider plant defenses via the synthesis of anti-microbial compounds and the resulting bacterial mortality. From a methodological point of view, the QSSA could be slightly

relaxed on the metabolites composing the xylem sap, which would allow for more dynamic and relevant modeling of the plant-pathogen interaction.

Using mathematical modeling to better understand bacterial wilt disease

Since 2016, several mathematical models have been developed to better understand the biology behind bacterial wilt disease. The first model, released in 2016, consisted of a high-quality metabolic network of *R. pseudosolanacearum* simulated in diverse *in vitro* environments using FBA (Peyraud et al., 2016). This model allowed measuring the ATP- equivalent cost of EPS synthesis and virulence. This metabolic network was subsequently interfaced with a regulatory network controlling multiple virulence factors and simulated across a broad set of environmental conditions using a discrete logical modeling method (Peyraud et al., 2018). The resulting model revealed that the virulence regulatory network exerts a control of the primary metabolism to promote robustness upon infection.

More recently, Baroukh et al. (2024) modeled the *in planta* population dynamics of *R. pseudosolanacearum* during tomato infection using a macroscopic modeling framework relying on Monod kinetics. This mathematical model predicted substrate consumption, putrescine production and biomass growth of *R. pseudosolanacearum*. Unlike previous models, it did not incorporate the metabolic network of *R. pseudosolanacearum* or its regulatory network, nor did it include the plant's metabolic network, which was simply modeled as a continuous environment providing substrate fluxes to the pathogen. Despite these simplifications, the model accurately reproduced experimental observations, including high bacterial densities and the depletion of glutamine and asparagine. Additionally, it estimated key parameters such as the bacterial mortality rate within the plant and the rate at which bacterial putrescine is assimilated by the plant.

In the present study, the metabolic networks of *R. pseudosolanacearum* and the tomato plant were merged, and the resulting model was simulated using sequential FBAs for diverse bacterial densities within the plant. The model demonstrated several key findings: i) the plant's photosynthetic capacity is the most critical factor for bacterial proliferation, ii) a reduction in plant transpiration limits and ultimately stops plant and pathogen growths, iii) hijacking stem resources, potentially through virulence factors,

448 can enhance bacterial growth but is not essential, and iv) pathogen-excreted
449 putrescine is predicted to be directly reused for plant biomass.

450 Another metabolic model of a plant-pathogen interaction was recently developed by
451 Rodenburg et al. (2019), representing the *Phytophthora infestans* - tomato leaf
452 pathosystem. This study differs from ours in several key aspects, as it employs a
453 qualitative approach, in contrast to our quantitative methodology. This difference is
454 evident in: i) the *P. infestans* biomass equation, which uses equal stoichiometric
455 coefficients, ii) the absence of mass conversion between plant and pathogen fluxes,
456 iii) the unrestricted uptake of all metabolites from tomato cell cytosol by the pathogen,
457 and iv) the lack of calibration for maximal uptake rates for both *P. infestans* and the
458 plant. Roderburg et al. (2019) also utilized a tomato leaf-centered model, which is
459 substantially less complex than our multi-organ model that incorporates a vascular
460 system, and the impact of *P. infestans* growth on plant metabolism and physiology was
461 not simulated. Indeed, all objective functions in their FBA simulations focused
462 exclusively on pathogen growth, whereas our model considers the interplay between
463 pathogen and plant growth.

464 In each of the Ralstonia mathematical models developed so far, different modeling
465 approaches have been used, different objects have been modeled, various
466 experimental data have been used for calibration, and distinct biological questions
467 have been addressed. Consequently, each model possesses its own specificity and
468 provides unique insights into the mechanisms at play during bacterial wilt disease.
469 Future directions could involve improving existing models by better representing the
470 plant putrescine degradation pathway and incorporating the synthesis of anti-microbial
471 compounds. Alternatively, models could be made more complex by considering the
472 spatial aspects of infection and representing the effects of abiotic and biotic conditions
473 of the plant on the pathosystem. Models incorporating plant immunity and its interaction
474 with *R. pseudosolanacearum* virulence factors could also be developed. It should be
475 noted the complexity of the events triggered by this interaction in both host and
476 pathogen makes such modeling challenging. An additional challenge lies in hybridizing
477 this type of model with metabolic models that use their own formalism adapted to
478 biochemical reactions. In this study, we focused on a relatively late stage of interaction
479 when the pathogen begins rapid multiplication in host tissues after successful entry
480 and establishment. We proposed a methodological framework that enabled the

481 creation of a first quantitative model of an antagonistic interaction at this specific phase.
482 While the model does not directly account for immunity and virulence mechanisms, it
483 successfully evaluated the impact of plant resource diversion by the pathogen. This
484 approach paves the way for developing more complex plant-bacteria interaction
485 models that explicitly integrate the interplay between metabolism, immunity and
486 virulence mechanisms.

487 Plant transpiration is the main factor leading to growth arrest of both 488 the host and the pathogen wilt disease

489 VIRION allowed to test and identify which physiological or environmental factors are
490 behind plant growth arrest and pathogen growth arrest during bacterial wilt disease.
491 First, our simulation results showed that the maximal carbon uptake capacity of the
492 plant (through photosynthesis), not nitrogen or iron, set the maximal plant density of
493 Ralstonia cells achievable (Figure 5). However, we also found that carbon, or any other
494 metabolic bottlenecks such as nitrogen and iron, are insufficient to explain the early
495 arrest of plant growth that was experimentally observed in Gerlin et al. (2021). To
496 explain this plant growth arrest, a physiological constraint was necessary: limiting
497 transpiration, impacting xylem fluxes and hence access to nutrients for the plant aerial
498 parts and later on the pathogen (Figure 5). Interestingly, at densities where this
499 transpiration-limitation is induced, the plant growth was affected immediately, in
500 agreement with experimental observations, contrary to the bacteria which continued to
501 thrive up to several logs higher. This underlines the pathogen's perfect metabolic
502 adaptation to this challenging environment.

503 Naturally, questions arise on the mechanism responsible of plant transpiration
504 decrease upon *R. pseudosolanacearum* presence in xylem vessels. Physical presence
505 of *Ralstonia* cells could impede xylem flow in itself, but an indirect mechanism such as
506 large bacterial exopolysaccharides excretion could also be responsible by making
507 xylem sap so viscous that it impedes its flow. To discriminate between these
508 hypotheses or others possible mechanisms, further investigation is necessary.

509 Stem resource hijacking, a strategy likely little used by *R.* 510 *pseudosolanacearum* during tomato infection

511 In literature, it is commonly described that xylem sap is nutrient-poor and cannot
512 sustain the biotrophic growth of a plant pathogen to high densities (De La Fuente et

513 al., 2022), thus requiring the bacterial pathogen to force the plant to release additional
514 nutrients, such as sugars (Hamilton et al., 2021; MacIntyre et al., 2020). However,
515 VIRION simulations, integrating both xylem concentrations and flow, tend to show that,
516 even with a transpiration limit, a moderate growth rate of *R. solanacearum* can be
517 reached up to 10^9 CFU/gFW solely through biotrophic growth, in agreement with
518 experimental observed values (Gerlin, Escourrou, et al., 2021). From 10^{10} CFU/gFW,
519 a growth rate is still present but very close to 0. Thus, xylem sap, when considered as
520 the product of a continuous flow, is not poor and very high bacterial densities can be
521 reached solely through biotrophic growth of the pathogen.

522 We then investigated how resource hijacking could contribute to *R.*
523 *pseudosolanacearum* growth. We confirmed by simulation that this mechanism could
524 theoretically be an effective pathogen strategy to boost its growth and compensate, for
525 example, the effect of transpiration decline, since it allowed the pathogen to have a
526 non-negligible growth rate up to 10^{10} CFU/gFW. We also confirmed that in the case of
527 stem resource hijacking, this would primarily involve sugars and some amino acids
528 (Figure 5). This would explain why Hamilton et al. (2021) reported a slight increase of
529 sugars in infected xylem sap. Nevertheless, we also showed that this mechanism is
530 probably dispensable for *R. pseudosolanacearum* since according to bacterial
531 population dynamics *in planta* experimentally measured in Gerlin et al. (2021),
532 pathogen growth almost stops around 10^9 CFU/gFW and not 10^{10} CFU/gFW. This also
533 aligns with the observation that mutants defective in sugar assimilation still fully wilt
534 tomato plants, with a slight delay (Hamilton et al., 2021; Gerlin, Escourrou, et al., 2021).
535 We thus conclude that hijacking plant resources from the stem is not likely to occur in
536 bacterial wilt or, if it does, the quantities of nutrients hijacked are much lower than the
537 maximal quantity that can be theoretically hijacked, as predicted by the model.
538 Reducing the amount of glutamine in the xylem sap, which is the major carbon source
539 for the bacterium, seems to be a better strategy for limiting the growth of *R.*
540 *pseudosolanacearum* in the plant. However, such modifications would likely affect
541 plant metabolism and phenotype even before impacting the pathogen, as our model
542 tends to indicate. Nevertheless, it might be worthwhile to consider how managing the
543 plant's environment, such as nutrition or watering, could mitigate xylem sap flow and
544 composition and thus minimize *Ralstonia* growth in the plant.

While *R. pseudosolanacearum* appears to favor a fast consumption of resources, as its metabolic and growth capacities outcompete those of the plant, other plant pathogen might not exhibit this behavior but instead favor a reduced growth in xylem vessels. In particular, *Xylella fastidiosa*, although capable of metabolizing various xylem sap components (Gerlin et al., 2020), has very limited growth rates *in vitro* and *in planta*, and is described as adopting a self-limiting behavior (Gerlin et al., 2020; Roper et al., 2019). In these conditions, the plant would be able to dominate the trophic interaction and limit bacterial spread. This suggests that these pathogens would favor a long stay in xylem vessels at low bacterial densities. In this case, a coexistence with the plant takes place in which the bacterium is not competing for resources, and both the plant and the pathogen can remain metabolically active.

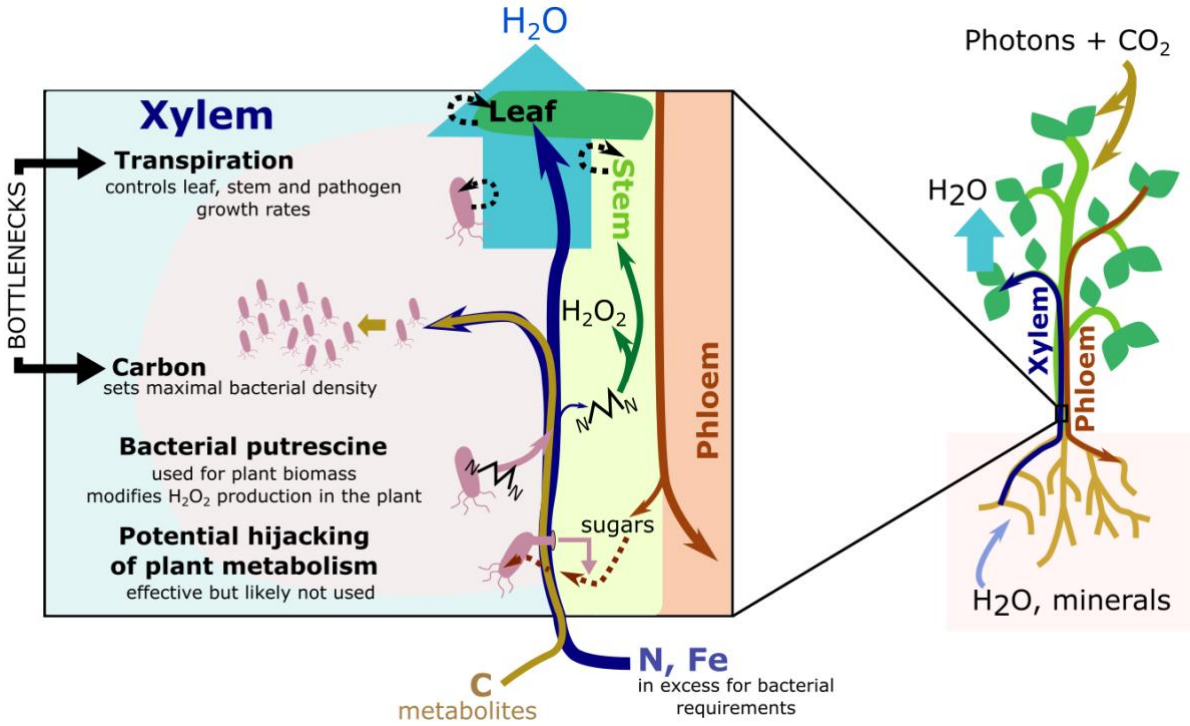

Figure 5: Key metabolic parameters during bacterial wilt at the origin of a successful infection. Decrease in transpiration during infection appears to be the most likely mechanism behind the cessation of plant growth and pathogen growth. Among diverse nutrients, carbon is the most limiting one for bacterial maximal density reachable. The study also showed that, although diverting nutrients from the phloem to the xylem via the stem is an effective strategy for increasing bacterial multiplication in plants, it is poorly used in the case of bacterial wilt. Finally, the effect of bacterial

putrescine production on host metabolism was shown to interfere with H_2O_2 synthesis in the plant, likely having an effect on ROS response.

Methods

Construction of VIRION

The cell tomato metabolic model from Gerlin et al., (2022) was used (SBML file) as a starting point. Reactions for iron, manganese, cobalt, molybdenum and zinc assimilation, which were not represented in the initial metabolic model, were added as these metabolites were necessary for predicting *R. pseudosolanacearum* growth using its genome-scale metabolic model (Peyraud et al., 2016). This addition, as well as other changes or improvements on putrescine metabolism and biomass are fully described in Supplementary Text 1. A multi-organ tomato model was generated using the same procedure as in Gerlin et al., (2022). Briefly, using an in-house script, the model was replicated into three models, representing leaf, stem and root with adequate biomass reaction for each organ. Exchange reactions, considering weight ratios between the different organs, were added to allow the exchange of metabolites between organs through xylem and phloem. Xylem represented exchanges between root and aerial parts, while phloem represented exchanges between aerial parts and roots. Stem could exchange in both directions with the phloem. Contrary to our previous multi-organ metabolic model, stem could uptake elements from the xylem but could not provide elements to this compartment, except when mentioned. As in Gerlin et al., (2022), a transport cost was added for each exchange reactions except for water. Different physiological constraints (uptakes of water and minerals by roots only, no photosynthesis for root, limited photosynthesis for stem) were integrated to model the different roles of each organ as in Gerlin et al., (2022).

The in-house scripts also merged *R. pseudosolanacearum* metabolic model taken from Peyraud et al. (2016) to the multi-organ model, generating a four-compartment model: leaf, stem, root, pathogen. The boundary metabolites were removed from the metabolic model of *R. pseudosolanacearum*, and external metabolites of the pathogen model were considered as xylem metabolites. To avoid dead-end metabolites, sink reactions were added allowing the exit of *R. pseudosolanacearum* metabolites excreted into the xylem and not present in healthy plant xylem sap. Simulations revealed very few sink reactions were used, and at very low fluxes. In addition, experimental data showed that few metabolites were enriched upon Ralstonia infection in xylem sap (Gerlin, Escourrou, et al., 2021; Lowe-Power et al., 2018). The weight

ratio between *R. pseudosolanacearum* and the plant was implemented in the exchange reactions between the xylem and the bacterial periplasm and were modified to represent the different bacterial densities. Conversion of *R. pseudosolanacearum* weight into colony forming unit (CFU) per g of fresh weight (FW) was estimated to follow 1 CFU/g stem FW = $1.10 \cdot 10^{-11}$ g bact / 1.52 g stem dry weight, based on: i) OD/CFU and OD/g ratios from Peyraud et al. (2016), ii) fresh weigh/dry weight (FW/DW) from Gerlin et al. (2022), iii) the leaf/stem and stem/root ratio in tomato metabolic model (Gerlin et al., 2022) which impose relative contents of 1.52 g stem DW and 3.37 g leaf DW for 1 g root DW (Supplementary Text 2).

Calibration of *R. pseudosolanacearum* metabolic model for growth *in planta*

To determine growth, excretion and assimilation capacities of *R. pseudosolanacearum* in the presence of xylem carbon sources, we used the data and model generated in Baroukh et al. (2024). In this study, a shake-flask growth experiment was performed in a minimal medium supplemented with a mixture of organic substrates whose relative concentrations mimics a tomato xylem. Growth, substrate assimilation and product excretion were monitored and used to determine uptake, excretion and growth rates among this combination of carbon sources. Glutamine and glucose assimilation followed Monod-type kinetics and were driving growth, while other substrate assimilation rates were proportional to the assimilation of glutamine and glucose. From the Monod kinetics, two maximal assimilation rates, one for glutamine and one for glucose, were implemented as a constraint bound in the model:

$$Gln_{ass_{rate}} \leq k_{gln} * \mu_{max_{gln}} * \frac{[Gln]}{[Gln] + K_{s_{gln}}} * 1000 * 24$$

$$Gluc_{ass_{rate}} \leq k_{gluc} * \mu_{max_{gluc}} * \frac{[Gluc]}{[Gluc] + K_{s_{gluc}}} * 1000 * 24$$

With:

- $Gln_{ass_{rate}}$ the assimilation rate of glutamine in the model (mmol·gB^{-1}·day^{-1}), k_{gln} (mmol·mgB^{-1}) the quantity of glutamine necessary to yield 1mg of biomass, $\mu\max_{gln}$ (h^{-1}) the maximal growth rate on glutamine, $K_{S_{gln}}$ (mM) the semi-saturation growth term on glutamine, $[Gln]$ (mM) the concentration of glutamine in tomato xylem sap

- $Gluc_{ass_{rate}}$ the assimilation rate of glucose in the model (mmol·gB^{-1}·day^{-1}), k_{gluc} (mmol·mgB^{-1}) the quantity of glucose necessary to yield 1g of biomass, $\mu\max_{gluc}$ (h^{-1}) the maximal growth rate on glucose, $K_{S_{gluc}}$ (mM) the semi-saturation growth term on glucose, $[Gluc]$ (mM) the concentration of glucose in tomato xylem sap

From each other substrate, to ensure assimilation only when glucose or glutamine were assimilated, a constraint proportional to glucose and glutamine rate was added:

$$os_{ass_{rate}} \leq \frac{k_{OS}}{k_{gln}} * Gln_{ass_{rate}} + \frac{k_{OS}}{k_{gluc}} * Gluc_{ass_{rate}}$$

With $os_{ass_{rate}}$ (mmol·gB^{-1}·day^{-1}) the assimilation rate of the other substrate (phenylalanine, valine, leucine, arginine, sucrose, tyrosine, proline, lysine, threonine, isoleucine, asparagine). All values were taken from Baroukh et al. (2024).

ATP maintenance was calibrated so that *R. pseudosolanacearum* growth rate prediction was in agreement with experimental data measured in Baroukh et al. (2024).

Sequential FBAs

Modeling of the interaction was performed using four successive FBAs with different objective functions.

1. Minimization of photon uptake

This first FBA is performed with leaf, stem and root growth rates constrained to experimental values, on the plant alone (VYTOP model). Minimizing photon uptake allowed acquiring the plant physiological capacities (photosynthesis, iron, nitrogen uptake) to ensure growth of a healthy plant in the absence of a pathogen.

2. Maximization of the pathogen biomass

The photon uptake rate determined in FBA 1 (representing healthy plant physiological capacities) was implemented as additional constraint, to avoid that the infected plant has a higher photosynthesis rate than a healthy plant. The leaf and stem growth rates were relaxed, to model the fact that *R. pseudosolanacearum* resource acquisition and proliferation will hinder the possibility of the aerial part of the plant to grow optimally, as observed experimentally (Gerlin, Escourrou, et al., 2021). Root growth rate remained constrained as we found in the experiments that root growth was not impacted by *R. pseudosolanacearum* (Gerlin, Escourrou, et al., 2021). The objective

660 function in this FBA was the maximization of the pathogen biomass reaction (i.e.
661 maximal proliferation). The result of the simulation was the maximal growth rate of *R.*
662 *pseudosolanacearum* constrained by the plant physiological capacities.

663 In this FBA, it was also possible to limit the nitrogen or iron uptake rate of the plant by
664 setting the upper bound the related transport reactions to the value obtained FBA 1. It
665 was also possible to limit transpiration. Measurements of transpiration during plant –
666 *R. pseudosolanacearum* interaction revealed a decrease of transpiration when the
667 pathogen is present at more than 10^7 CFU per g of stem fresh weight (FW) (Gerlin,
668 Escourrou, et al., 2021). We estimated thanks to a linear regression a transpiration
669 decrease linear rule, depending on the bacterial density (in decimal logarithm):
670 t*ranspiration reduction coefficient = -0.2746* [log*$_{10}$ *CFU/gFW] + 2.8764*. As xylem
671 fluxes of matter depend on the transpiration rate, the upper bound of xylem fluxes was
672 constrained by this transpiration reduction coefficient if the bacterial density was more
673 than 10^7 CFU/gFW.

674 3. Maximization of the growth of the aerial parts

675 In this FBA, the pathogen growth rate was now considered as an additional constraint,
676 and leaf/stem biomass reactions were maximized. To this end, maximization of leaf
677 biomass reaction flux was set as objective, and a constant ratio between leaf and stem
678 biomass was imposed to ensure balanced growth of both the stem and the leaves.
679 This FBA determined the growth of the aerial parts still achievable in the presence of
680 *R. pseudosolanacearum*, as the pathogen deprived the plant from a part of its nutrients.

681 4. Minimization of the sum of absolute fluxes

682 In this FBA, the leaf/stem growth rates obtained from FBA 3 were set as additional
683 constraints and minimization of all the fluxes was performed. This allowed to consider
684 a parsimonious enzyme usage in both organisms as well as avoid the presence of
685 Stoichiometric Balanced Cycles. This FBA was similarly performed as for the plant
686 model alone (Gerlin et al., 2022).

687 **Software requirements**

688 Simulations were performed with Python 3 scripts, the open access libraries lxml,
689 pandas and the linear programming solver CPLEX Python API, developed by IBM. The
690 scripts used to perform all the simulations, as well as the genome-scale metabolic

models, can be found on Github at this link: https://github.com/cbaroukh/VIRION [released once accepted].

An academic or commercial license of CPLEX Python API (ILOG CPLEX Optimization Studio) is mandatory to run the scripts. The academic license is free for academic institutions. The basic “free Community Edition” version of CPLEX is not suitable and will provide an error message.

Data availability

All data supporting the findings of this study are available within the paper and within its supplementary materials. The scripts used to perform all the simulations, as well as the genome-scale metabolic models, can be found on Github at this link: https://github.com/cbaroukh/VIRION [released once accepted].

Author contributions

Caroline Baroukh: Conceptualization (lead); Data curation (equal); Formal analysis (equal); Funding acquisition (lead); Investigation (equal); Methodology (equal); Project administration (lead); Resources (equal); Supervision (lead); Writing – original draft (supporting); Writing – review and editing (equal).

Léo Gerlin: Data curation (equal); Formal analysis (equal); Methodology (equal); Investigation (equal); Writing – original draft (lead); Writing – review and editing (equal).

Stéphane Genin: Conceptualization (supporting); Methodology (supporting); Resources (equal); Writing – review and editing (equal).

Competing interest statement

The authors declare no competing interests.

Funding statement

Léo Gerlin was funded by a PhD grant from the French Ministry of National Education and Research. The study was funded by the French Laboratory of Excellence (LABEX) project TULIP (ANR-10-LABX-41 and ANR11-IDEX-0002-02). The funders had no role in study design, data collection and analysis, decision to publish, or preparation of the manuscript.

722 ## Supplementary data

723 **Supplementary Table 1**

724 Experimental constraints used to calibrate the multi-organism metabolic model.

725 **Supplementary Figure 1**

726 *R. pseudosolanacearum* uptake rates depending on the bacterial density and the
727 limiting factors. g: g of *R. pseudosolanacearum* dry weight. CFU: colony forming units.

728 **Supplementary Text 1**

729 Modifications of tomato metabolic model to build a whole plant – pathogen model.

730 **Supplementary Text 2**

731 Integration of bacterial density in VIRION.

732

References

Abu Kwaik, Y., & Bumann, D. (2013). Microbial quest for food *in vivo* : 'Nutritional virulence' as an emerging paradigm: Microbial nutritional virulence. *Cellular Microbiology*, *15*(6), 882-890. https://doi.org/10.1111/cmi.12138

Baroukh, C., Gerlin, L., Escourrou, A., & Genin, S. (2024). Unraveling the in planta population dynamics of the plant pathogen Ralstonia pseudosolanacearum by mathematical modeling. *New Phytologist*. https://doi.org/10.1111/nph.20216

Baroukh, C., Zemouri, M., & Genin, S. (2022). Trophic preferences of the pathogen *Ralstonia solanacearum* and consequences on its growth in xylem sap. *MicrobiologyOpen*, *11*(1), e1240. https://doi.org/10.1002/mbo3.1240

Berger, S., Sinha, A. K., & Roitsch, T. (2007). Plant physiology meets phytopathology : Plant primary metabolism and plant pathogen interactions. *Journal of Experimental Botany*, *58*(15-16), 4019-4026. https://doi.org/10.1093/jxb/erm298

Bhatt, G., & Denny, T. P. (2004). *Ralstonia solanacearum* Iron Scavenging by the Siderophore Staphyloferrin B Is Controlled by PhcA, the Global Virulence Regulator. *Journal of Bacteriology*, *186*(23), 7896-7904. https://doi.org/10.1128/JB.186.23.7896-7904.2004

Bialczyk, J., Lechowski, Z., & Dziga, D. (2004). Composition of the xylem sap of tomato seedlings cultivated on media with HCO_3^- and nitrogen source as NO_3 <sup/>—Or NH_4^+. *Plant and Soil*, *263*(1), 265-272. https://doi.org/10.1023/B:PLSO.0000047739.11698.ca

Dalsing, B. L., & Allen, C. (2014). Nitrate Assimilation Contributes to Ralstonia solanacearum Root Attachment, Stem Colonization, and Virulence. *Journal of Bacteriology*, *196*(5), 949-960. https://doi.org/10.1128/JB.01378-13

Dalsing, B. L., Truchon, A. N., Gonzalez-Orta, E. T., Milling, A. S., & Allen, C. (2015). Ralstonia solanacearum Uses Inorganic Nitrogen Metabolism for Virulence, ATP Production, and Detoxification in the Oxygen-Limited Host Xylem Environment. *mBio*, *6*(2), e02471-14. https://doi.org/10.1128/mBio.02471-14

De La Fuente, L., Merfa, M. V., Cobine, P. A., & Coleman, J. J. (2022). Pathogen Adaptation to the Xylem Environment. *Annual Review of Phytopathology*, *60*(1), 163-186. https://doi.org/10.1146/annurev-phyto-021021-041716

DeFalco, T. A., & Zipfel, C. (2021). Molecular mechanisms of early plant pattern-triggered immune signaling. *Molecular Cell*, *81*(17), 3449-3467. https://doi.org/10.1016/j.molcel.2021.07.029

diCenzo, G. C., Tesi, M., Pfau, T., Mengoni, A., & Fondi, M. (2020). Genome-scale metabolic reconstruction of the symbiosis between a leguminous plant and a nitrogen-fixing bacterium. *Nature Communications*, *11*(1), 2574. https://doi.org/10.1038/s41467-020-16484-2

Gerlin, L., Baroukh, C., & Genin, S. (2021). Polyamines : Double agents in disease and plant immunity. *Trends in Plant Science*, *26*(10), 1061-1071. https://doi.org/10.1016/j.tplants.2021.05.007

Gerlin, L., Cottret, L., Cesbron, S., Taghouti, G., Jacques, M.-A., Genin, S., & Baroukh, C. (2020). Genome-Scale Investigation of the Metabolic Determinants Generating Bacterial Fastidious Growth. *mSystems*, *5*(2), e00698-19. https://doi.org/10.1128/mSystems.00698-19

Gerlin, L., Cottret, L., Escourrou, A., Genin, S., & Baroukh, C. (2022). A multi-organ metabolic model of tomato predicts plant responses to nutritional and genetic perturbations. *Plant Physiology*, *188*(3), 1709-1723. https://doi.org/10.1093/plphys/kiab548

Gerlin, L., Escourrou, A., Cassan, C., Maviane Macia, F., Peeters, N., Genin, S., & Baroukh, C. (2021). Unravelling physiological signatures of tomato bacterial wilt and xylem metabolites exploited by *Ralstonia solanacearum*. *Environmental Microbiology*, *23*(10), 5962-5978. https://doi.org/10.1111/1462-2920.15535

Gerlin, L., Frainay, C., Jourdan, F., Baroukh, C., & Prigent, S. (2021). Plant genome-scale

metabolic networks. In *Advances in Botanical Research* (Vol. 98, p. 237-270). Elsevier. https://doi.org/10.1016/bs.abr.2020.09.021

Gu, C., Kim, G. B., Kim, W. J., Kim, H. U., & Lee, S. Y. (2019). Current status and applications of genome-scale metabolic models. *Genome Biology*, *20*(1), 121. https://doi.org/10.1186/s13059-019-1730-3

Hamilton, C. D., Steidl, O. R., MacIntyre, A. M., Hendrich, C. G., & Allen, C. (2021). *Ralstonia solanacearum* Depends on Catabolism of Myo-Inositol, Sucrose, and Trehalose for Virulence in an Infection Stage–Dependent Manner. *Molecular Plant-Microbe Interactions®*, *34*(6), 669-679. https://doi.org/10.1094/MPMI-10-20-0298-R

Herms, D. A., & Mattson, W. J. (1992). The Dilemma of Plants : To Grow or Defend. *The Quarterly Review of Biology*, *67*(3), 283-335. https://doi.org/10.1086/417659

Ingel, B., Caldwell, D., Duong, F., Parkinson, D. Y., McCulloh, K. A., Iyer-Pascuzzi, A. S., McElrone, A. J., & Lowe-Power, T. M. (2022). Revisiting the Source of Wilt Symptoms : X-Ray Microcomputed Tomography Provides Direct Evidence That *Ralstonia* Biomass Clogs Xylem Vessels. *PhytoFrontiers™*, *2*(1), 41-51. https://doi.org/10.1094/PHYTOFR-06-21-0041-R

Jian, Y., Gong, D., Wang, Z., Liu, L., He, J., Han, X., & Tsuda, K. (2023). How plants manage pathogen infection. *EMBO Reports*, *25*(1), 31-44. https://doi.org/10.1038/s44319-023-00023-3

Lacrampe, N., Lugan, R., Dumont, D., Nicot, P. C., Lecompte, F., & Colombié, S. (2024). Modelling metabolic fluxes of tomato stems reveals that nitrogen shapes central metabolism for defence against *Botrytis cinerea*. *Journal of Experimental Botany*, *75*(13), 4093-4110. https://doi.org/10.1093/jxb/erae140

Landry, D., González-Fuente, M., Deslandes, L., & Peeters, N. (2020). The large, diverse, and robust arsenal of *Ralstonia solanacearum* type III effectors and their in planta functions. *Molecular Plant Pathology*, *21*(10), 1377-1388. https://doi.org/10.1111/mpp.12977

Lowe-Power, T. M., Hendrich, C. G., Von Roepenack-Lahaye, E., Li, B., Wu, D., Mitra, R., Dalsing, B. L., Ricca, P., Naidoo, J., Cook, D., Jancewicz, A., Masson, P., Thomma, B., Lahaye, T., Michael, A. J., & Allen, C. (2018). Metabolomics of tomato xylem sap during bacterial wilt reveals *Ralstonia solanacearum* produces abundant putrescine, a metabolite that accelerates wilt disease. *Environmental Microbiology*, *20*(4), 1330-1349. https://doi.org/10.1111/1462-2920.14020

Lowe-Power, T. M., Khokhani, D., & Allen, C. (2018). How Ralstonia solanacearum Exploits and Thrives in the Flowing Plant Xylem Environment. *Trends in Microbiology*, *26*(11), 929-942. https://doi.org/10.1016/j.tim.2018.06.002

Macho, A. P. (2016). Subversion of plant cellular functions by bacterial type- III effectors : Beyond suppression of immunity. *New Phytologist*, *210*(1), 51-57. https://doi.org/10.1111/nph.13605

MacIntyre, A. M., Barth, J. X., Pellitteri Hahn, M. C., Scarlett, C. O., Genin, S., & Allen, C. (2020). Trehalose Synthesis Contributes to Osmotic Stress Tolerance and Virulence of the Bacterial Wilt Pathogen *Ralstonia solanacearum*. *Molecular Plant-Microbe Interactions®*, *33*(3), 462-473. https://doi.org/10.1094/MPMI-08-19-0218-R

Orth, J. D., Thiele, I., & Palsson, B. Ø. (2010). What is flux balance analysis? *Nature Biotechnology*, *28*(3), 245-248. https://doi.org/10.1038/nbt.1614

Peyraud, R., Cottret, L., Marmiesse, L., & Genin, S. (2018). Control of primary metabolism by a virulence regulatory network promotes robustness in a plant pathogen. *Nature Communications*, *9*(1), 418. https://doi.org/10.1038/s41467-017-02660-4

Peyraud, R., Cottret, L., Marmiesse, L., Gouzy, J., & Genin, S. (2016). A Resource Allocation Trade-Off between Virulence and Proliferation Drives Metabolic Versatility in the Plant Pathogen Ralstonia solanacearum. *PLoS Pathogens*, *12*(10), e1005939. https://doi.org/10.1371/journal.ppat.1005939

Pfau, T., Christian, N., Masakapalli, S. K., Sweetlove, L. J., Poolman, M. G., & Ebenhöh, O. (2018). The intertwined metabolism during symbiotic nitrogen fixation elucidated by metabolic modelling. *Scientific Reports*, *8*(1), 12504. https://doi.org/10.1038/s41598-018-30884-x

Rodenburg, S. Y. A., Seidl, M. F., Judelson, H. S., Vu, A. L., Govers, F., & De Ridder, D. (2019). Metabolic Model of the *Phytophthora infestans* -Tomato Interaction Reveals Metabolic Switches during Host Colonization. *mBio*, *10*(4), e00454-19. https://doi.org/10.1128/mBio.00454-19

Roper, C., Castro, C., & Ingel, B. (2019). Xylella fastidiosa : Bacterial parasitism with hallmarks of commensalism. *Current Opinion in Plant Biology*, *50*, 140-147. https://doi.org/10.1016/j.pbi.2019.05.005

Vailleau, F., & Genin, S. (2023). *Ralstonia solanacearum* : An Arsenal of Virulence Strategies and Prospects for Resistance. *Annual Review of Phytopathology*, *61*(1), 25-47. https://doi.org/10.1146/annurev-phyto-021622-104551

Walters, D., & Heil, M. (2007). Costs and trade-offs associated with induced resistance. *Physiological and Molecular Plant Pathology*, *71*(1-3), 3-17. https://doi.org/10.1016/j.pmpp.2007.09.008

Windram, O., Penfold, C. A., & Denby, K. J. (2014). Network Modeling to Understand Plant Immunity. *Annual Review of Phytopathology*, *52*(1), 93-111. https://doi.org/10.1146/annurev-phyto-102313-050103

Yuan, H., Cheung, C. Y. M., Poolman, M. G., Hilbers, P. A. J., & Van Riel, N. A. W. (2016). A genome-scale metabolic network reconstruction of tomato (*Solanum lycopersicum* L.) and its application to photorespiratory metabolism. *The Plant Journal*, *85*(2), 289-304. https://doi.org/10.1111/tpj.13075

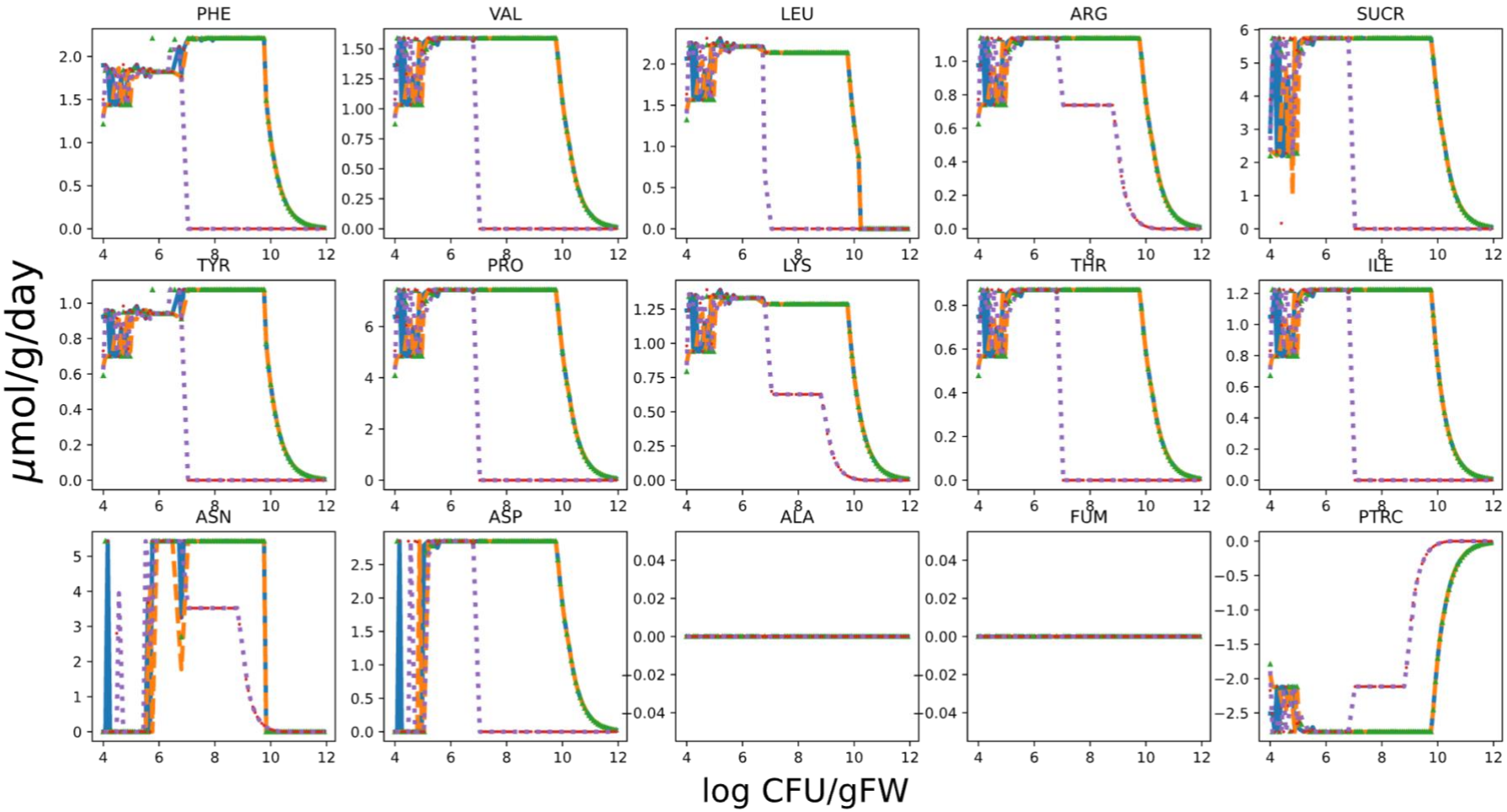

Supplementary Figure 1: *R. pseudosolanacearum* uptake rates depending on the bacterial density and the limiting factors. g: g of *R. pseudosolanacearum* dry weight. CFU: colony forming units.

859 **Supplementary Table 1**

860 Experimental constraints used to calibrate the multi-organism metabolic model.

Variable	Constraint	Value	Note	References
leaf growth rate (day^{-1})	Lower bound	0.21		https://doi.org/10.1093/plphys/kiab548
stem growth rate (day^{-1})	Lower bound	0.26		https://doi.org/10.1093/plphys/kiab548
root growth rate (day^{-1})	Lower bound	0.17		https://doi.org/10.1093/plphys/kiab548
organic uptake, pathogen (mmol/g/day)	Upper bound	value in the macroscopic model of Ralstonia		https://doi.org/10.1111/nph.20216
pathogen:plant ratio (cells per g of plant fresh weight)	Stoichiometric coefficient between plant and xylem, and xylem and pathogen	10^4 - 10^{12}	Range of experimentally plausible values, based on experimental measurements	https://doi.org/10.1111/1462-2920.15535

transpiration reduction	Upper bound of 'root to xylem' exchange fluxes	*(-0.2746* [log_{10} CFU/gFW] + 2.8764)* of uninfected root to xylem flux from FBA 1		https://doi.org/10.1111/1462-2920.15535
leaf:stem ratio (g/g)	Stoichiometric coefficient between leaf and stem biomass fluxes	2.2	To allow both leaf and stem biomass maximization in FBA 3	https://doi.org/10.1093/plphys/kiab548

861

862

Supp Text 1

Modifications of tomato metabolic model to build a whole plant – pathogen model

1. Determination of iron concentration in tomato plant from literature for integration in biomass

Iron was initially absent from tomato biomass. Regarding its importance in plant – *Ralstonia* interaction (ref), we added it to organ biomass reactions (R_BIOMASS_ROOT, R_BIOMASS_STEM, R_BIOMASS_LEAF). We determined the coefficient value in the equation following the procedure below.

- **From Twyman, 1959 [1]**

Mean concentration of iron in dry leaf tissue of tomato plants:
[Fe] = 144 ppm at the highest iron supply (Table 2)
[Fe] = 144 ppm = 144 mg Fe/kg leaf DW

Note: at the lowest iron supply, the value remains close (112 mg Fe/kg leaf DW).

- **From Carpena et al., 1988 [2]**

Cultivar	Vermone	Marglobe
Nutrient consumption (mg Fe/plant) – Table 3	301	298
Yield, plant weight (g/plant) – Table 4	3054	2613
Yield, fruit weight (g/plant) – Table 4	6648	3930
Yield, plant dry weight (g DW/plant)*	432	370
Yield, fruit dry weight (g DW/plant)**	398	235
Total dry weight (g DW/plant)	830	605
Total dry weight (kg DW/plant)	0.830	0.733
[Fe] (mg Fe/kg DW)* **	**363**	**406.5**

*Using FW/DW ratio of 7.07 according to Gerlin et al., 2022 [3]

**Using FW/DW ratio of 16.7 (6% of dry content) [4]

***[Fe] (mg Fe/kg DW) = Nutrient consumption (mg Fe/plant)/Total dry weight (kg DW/plant)

➔ Integration of iron concentration in tomato model

The range estimated from literature is **144 – 406.5 mg Fe/kg DW** in a tomato plant.
Biomass equation represents 1 g of organ DW, corresponding to 1.44 – 4.07 10^{-4} g Fe.
Using the atomic weight of Fe (55.845 g/mol), it represents 2.58 – 7.28 10^{-6} mol Fe.
Biomass equation is expressed in µmol/gDW, so the range of values to integrate in the model is: **2.58 – 7.28 µmol/gDW.** Iron is majorly found in and between plant organs as Fe2+ (M_fe2_c) [5], so iron will be incorporated in biomass equation as M_fe2_c (see reference below).
Here, we do not take into account the organ specificity of iron concentration and add the same value in leaf, stem and root. We integrate the highest value to mimic a maximal requirement. Simulations presented in the paper show that even this high value has poor impact on the interaction.

2. Addition of minerals required for pathogen growth

Molybdate (M_mobd_c), manganese (M_mn_c) and cobalt (M_cobalt_c) are present in *R. pseudosolanacearum* biomass equation while they were not modeled in plant initial metabolic model (Sl2183).
We added:

- **For molybdate**

The internal metabolite M_mobd_c was already present. We added the boundary metabolite M_mobd_b and the uptake reaction R_EX_mobd_c, written as follow:
M_mobd_b <-> M_mobd_c

- **For manganese**

We added the internal and boundary metabolites M_mn2_b and M_mn2_c and the uptake reaction R_EX_mn2_c, written as follow:
M_mn2_b <-> M_mn2_c

- **For cobalt**

We added the internal and boundary metabolites M_cobalt2_b and M_cobalt2_c and the uptake reaction R_EX_cobalt2_c, written as follow:
M_ cobalt2_b <-> M_ cobalt2_c

3. Corrections of amino acid coefficients in biomass equation

The coefficients for some amino acids were inverted in the previous files of tomato model published in 2022 [3]. While it does not have significant impact on the simulations, either here or in the previous work, we rewrote the coefficients for the following amino acids: M_cys__L_c, M_ala__B_c, M_his__L_c, M_ile__L_c, M_leu__L_c, M_lys__L_c with the correct values from the list of biomass components (Supp File 1 of Gerlin et al. 2022 [3], sheets 3, 4, 5).

4. Putrescine metabolism

We manually examined putrescine catabolism in Sl2183, as our initial model was not representing putrescine catabolism. We looked at canonical putrescine catabolism in plants in literature [6] and databases (https://pmn.plantcyc.org/pathway?orgid=ARA&id=PWY-2).
We found that the first reaction of putrescine catabolism, putrescine oxidase* (EC 1.4.3.10) was already included in our model (converting putrescine into 4-aminobutanoate), but we missed the following reaction, aminobutyraldehyde dehydrogenase** (EC 1.2.1.19), converting 4-aminobutanoate into GABA. We found two orthologs (SOLYC06G071290 OR SOLYC03G113800) to the A. thaliana gene (ALDH10A9 / AT3G48170) annotated as aminobutyraldehyde dehydrogenase in BioCyc. This provides evidence for the completeness of the pathway in tomato, and we thus added aminobutyraldehyde dehydrogenase in the modeL

*Putrescine oxidase
R_PTRCOX1 http://bigg.ucsd.edu/universal/reactions/PTRCOX1 in BiGG
PUTRESCINE-OXIDASE-RXN https://biocyc.org/reaction?orgid=META&id=PUTRESCINE-OXIDASE-RXN in BioCyc
Reaction in BiGG: M_h2o_c + M_o2_c + M_ptrc_c -> M_4abutn_c + M_h2o2_c + M_nh4_c

**Aminobutyraldehyde dehydrogenase
R_ABUTD http://bigg.ucsd.edu/models/iJO1366/reactions/ABUTD in BiGG
AMINOBUTDEHYDROG-RXN https://biocyc.org/reaction?orgid=META&id=AMINOBUTDEHYDROG-RXN in BioCyc
Reaction in BiGG: M_4abutn_c + M_h2o_c + M_nad_c -> M_4abut_c + 2.0 M_h_c + M_nadh_c

References

[1] E. S. Twyman, « The effect of iron supply on the yield and composition of leaves of tomato plants », *Plant Soil*, vol. 10, nº 4, p. 375-388, avr. 1959, doi: 10.1007/BF01666211.
[2] O. Carpena, A. Masaguer, et M. J. Sarro, « Nutrient uptake by two cultivars of tomato plants », *Plant Soil*, vol. 105, nº 2, p. 294-296, sept. 1988, doi: 10.1007/BF02376796.
[3] L. Gerlin, L. Cottret, A. Escourrou, S. Genin, et C. Baroukh, « A multi-organ metabolic model of tomato predicts plant responses to nutritional and genetic perturbations », *Plant Physiol.*, vol. 188, nº 3, p. 1709-1723, mars 2022, doi: 10.1093/plphys/kiab548.
[4] E. Cozzolino *et al.*, « Effects of the Application of a Plant-Based Compost on Yield and Quality of Industrial Tomato (Solanum lycopersicum L.) Grown in Different Soils », *Appl. Sci.*, vol. 13, nº 14, p. 8401, juill. 2023, doi: 10.3390/app13148401.
[5] J.-F. Briat, C. Curie, et F. Gaymard, « Iron utilization and metabolism in plants », *Curr. Opin. Plant Biol.*, vol. 10, nº 3, p. 276-282, juin 2007, doi: 10.1016/j.pbi.2007.04.003.
[6] R. Rastogi et P. J. Davies, « Polyamine Metabolism in Ripening Tomato Fruit 1: I. Identification of Metabolites of Putrescine and Spermidine », *Plant Physiol.*, vol. 94, nº 3, p. 1449-1455, nov. 1990, doi: 10.1104/pp.94.3.1449.

Supp Text 2

Integration of bacterial density in VIRION

Numerical values used

$1.0157 \cdot 10^{12}$ CFU *Rs*/L = 1 OD	Value from (Peyraud et al., 2016) Linear regression from S4 Table.
0.414 g *Rs*/L = 1 OD	Value from (Peyraud et al., 2016) Materials and Methods.
g fresh weight / g dry weight [*Sl* stem] = 17.7	Value from (Gerlin et al., 2022) Figure 2.

g / CFU [*Rs*] = 0.414 g *Rs*/L / $1.0157 \cdot 10^{12}$ CFU *Rs*/L = $4.076 \cdot 10^{-13}$

1 cfu/g stem FW = 1·(g fresh weight / g dry weight [*Sl* stem]) = 17.7 **cfu/g stem DW**

In VYTOP model, the relative proportions are: 1.52 g stem DW and 3.37 g leaf DW for 1 g root DW. The bacterial density must be determined for 1.52 g stem DW.

1 cfu/g stem FW = 1.52 · 17.7 **cfu/1.52 g stem DW** = 26.904 **cfu/1.52 g stem DW**
1 cfu/g stem FW = 26.904 · (g / CFU [*Rs*]) **g bact / 1.52 g stem DW**
1 cfu/g stem FW = $26.904 \cdot 4.076.10^{-13}$ **g bact / 1.52 g stem DW**
1 cfu/g stem FW = $1.10 \cdot 10^{-11}$ **g bact / 1.52 g stem DW**

Rs: *Ralstonia pseudosolanacearum* GMI1000
Sl: *Solanum lycopersicum* M80

References

Peyraud R, Cottret L, Marmiesse L, Gouzy J, Genin S. A Resource Allocation Trade-Off between Virulence and Proliferation Drives Metabolic Versatility in the Plant Pathogen Ralstonia solanacearum. PLoS Pathog. 2016 Oct 12;12(10):e1005939. doi: 10.1371/journal.ppat.1005939. PMID: 27732672; PMCID: PMC5061431.

Gerlin L, Cottret L, Escourrou A, Genin S, Baroukh C. A multi-organ metabolic model of tomato predicts plant responses to nutritional and genetic perturbations. Plant Physiol. 2022 Mar 4;188(3):1709-1723. doi: 10.1093/plphys/kiab548. PMID: 34907432; PMCID: PMC8896645.